Prominent Short-Circuit Currents of Fluorinated Quinoxaline-Based Copolymer Solar Cells with a Power Conversion Efficiency of 8.0%

ARTICLE *in* CHEMISTRY OF MATERIALS · DECEMBER 2012

Impact Factor: 8.35 · DOI: 10.1021/cm302861s

6 AUTHORS, INCLUDING:

Hsieh-Chih Chen
National Central University
20 PUBLICATIONS **523** CITATIONS

SEE PROFILE

Shang-Wei Chou
National Taiwan University
19 PUBLICATIONS **578** CITATIONS

SEE PROFILE

CHEMISTRY OF MATERIALS

Article

pubs.acs.org/cm

Prominent Short-Circuit Currents of Fluorinated Quinoxaline-Based Copolymer Solar Cells with a Power Conversion Efficiency of 8.0%

Hsieh-Chih Chen,*[,†,‡] Ying-Hsiao Chen,[†,‡] Chi-Chang Liu,[†] Yun-Chen Chien,[†] Shang-Wei Chou,[†,‡] and Pi-Tai Chou*[,†,‡]

[†]Department of Chemistry, National Taiwan University, Taipei 10617, Taiwan, Republic of China

[‡]Center of Emerging Material and Advanced Devices, National Taiwan University, Taipei 10617, Taiwan, Republic of China

Supporting Information

ABSTRACT: A tailor-made medium-band gap fluorinated quinoxaline-based conjugated polymer of **PBDT-TFQ** was designed and synthesized as a donor material for bulk-heterojunction (BHJ) solar cells. This polymer is possessed of an intrachain donor−acceptor architecture and exhibits a broad and strong absorption spectrum across the entire UV−vis region. The introduction of F atoms with high electron affinity to the quinoxaline moiety is effective in further lowering both the highest occupied molecular orbital (HOMO) and the lowest unoccupied molecular orbital (LUMO) energy levels of **PBDT-TFQ** to attain higher open-circuit voltage (V_{oc}). With an optimized blend ratio of **PBDT-TFQ**:$PC_{71}BM$ (1:1, w/w), a high power conversion efficiency (PCE) of 8.0% was obtained, with a V_{oc} of 0.76 V, a short-circuit current density (J_{sc}) of 18.2 mA cm^{-2}, and a fill factor (FF) of 58.1% under AM 1.5G irradiation. The resulting copolymer reveals an outstanding J_{sc} value, arising from the higher hole mobility of **PBDT-TFQ**, together with the better continuous percolation pathways within the polymer blend for efficient exciton dissociation and charge transport.

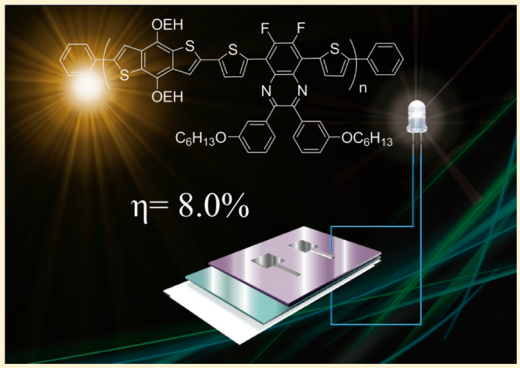

KEYWORDS: *solar cells, photovoltaic, quinoxaline, semiconductor, bulk heterojunction*

INTRODUCTION

In the past few decades, extensive efforts have been directed at developing solution-processed polymer solar cells (PSCs), because of their potential for being lightweight, having flexibility, and being used in low-cost energy harvesting.[1−3] So far, the most efficient architecture of PSCs is upon the donor−acceptor (D-A) bulk-heterojunction (BHJ) structure with a three-dimensional interpenetrating network of conjugated polymers blended with soluble fullerene derivatives[1−4] or nanocrystals.[5] PSC performance has significantly advanced in the past few years through the design and synthesis of novel conjugated polymers, modified interfacial layers,[6] optimized film morphologies,[7] and engineered device architectures.[6a,8] In addition, increasing the molecular weight of conjugated polymers has also demonstrated an improvement in PSC performance via promotion of hole mobility, optical property, and film morphology.[1d,3c,e] Moreover, alternating electron D and A subunits in polymer main chains has been an important strategy in designing high-performance polymers for PSC applications, because intramolecular charge transfer (ICT) from an electron-donating unit to an electron-withdrawing moiety within the fundamental repeat unit allows facile tuning of band gaps, frontier molecular orbital energies, and light absorption strength.[9] Therefore, remarkably more incident photons can be harvested for efficient charge carrier generation. Based on this tactic, the power conversion efficiencies (PCEs) of PSCs surpassing 7% under AM1.5G illumination have recently been reported.[1b,10]

Central to the electron donor unit, the benzo[1,2-*b*:4,5-*b*′]-dithiophene (BDT) has emerged as an attractive building block for BHJ solar cells due to its rigidity, coplanarity by fusing a benzene with two flanking thiophene units, high hole mobility, extremely extended π-conjugated structures, and proper side chain patterns for enhanced solubility.[11] Recently, a variety of compounds in terms of BDT-based copolymer family, which absorb more light by fine-tuning energy levels of polymers to better match their band gaps with the solar spectrum, have achieved substantial PCEs of 4%−7% when copolymerized with various electron acceptors, including benzothiadiazole (BT),[10b,c] thienothiophene (TT),[3a,10a,f] diketopyrrolopyrrole (DPP),[12a] thiazolothiazole (TTZ),[3b,d] and thienopyrroledione (TPD)[12b] derivatives. Recently, the incorporation of an electron-withdrawing F atom onto the periphery of A is attractive, since its small size is expected to minimize the undesired steric interactions, and its strong electron-affinity nature is also expected to stabilize the HOMO and LUMO energy levels.[14] Furthermore, fluorination also causes a decrease in the band gap in solid state, arising from the fact that the

Received: September 5, 2012
Revised: December 1, 2012
Published: December 4, 2012

Scheme 1. Synthetic Route Adopted for the Preparation of Monomers and Polymers[a]

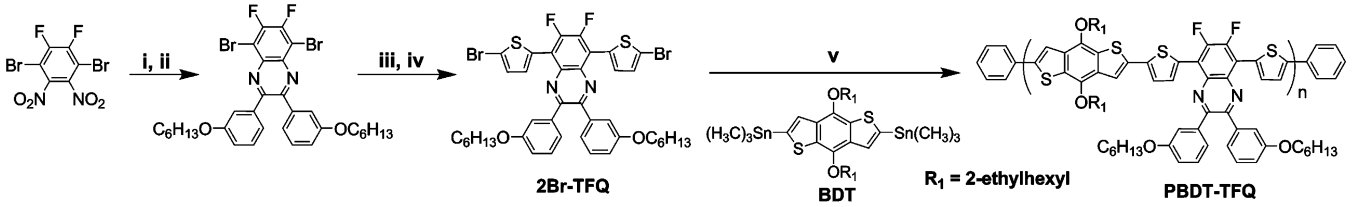

[a]The reagents and conditions: (i) Fe, AcOH, 50 °C, 4 h; (ii) 1,2-bis(3-hexyloxyphenyl)ethane-1,2-dione, AcOH, reflux, overnight; (iii) 2-(tributylstannyl)thiophene, $PdCl_2(PPh_3)_2$, toluene, reflux, 24 h; (iv) NBS, DMF, 30 °C, 8 h; and (v) $Pd(PPh_3)_4$, toluene, reflux, 72 h.

improvement in planarization of the conjugated backbone through favorable F-atom-induced intramolecular and/or intermolecular interactions.[10a,b,14]

In this regard, we report a straightforward synthetic methodology to prepare a new D-A alternating copolymer, namely, poly{4,8-bis(2′-ethylhexyloxy)-benzo[1,2-*b*:4,5-*b*′]-dithiophene-*alt*-[5,8-bis(5′-thiophen-2′-yl)-6,7-difluoro-2,3-bis-(3″-hexyloxyphenyl) quinoxaline]} (**PBDT-TFQ**; see Scheme 1), which turns out to be a very promising candidate for high-performance solar cells. This polymer, designed based on the intrachain D-A copolymer motif, was expected to exhibit a broad absorption spectrum. In addition, the introduction of F atoms with high electron affinity to the quinoxaline moiety is effective in further lowering both the highest occupied molecular orbital (HOMO) and the lowest unoccupied molecular orbital (LUMO) levels of **PBDT-TFQ** to attain higher open-circuit voltage (V_{oc}), short-circuit current density (J_{sc}), and PCE.[1b,3a,10a,b,14] A high PCE of up to 8.0% has been achieved with a blend ratio of 1:1 **PBDT-TFQ**:$PC_{71}BM$.

EXPERIMENTAL SECTION

Measurement and Characterization. Detailed experimental procedures for the synthesis and characterization of the **PBDT-TFQ** copolymer are given in the Supporting Information. ^1H, ^{13}C, and ^{19}F NMR spectra were recorded on a Varian Mercury 400. Mass spectra were obtained on a Finnigan LCQ mass spectrometer. Chemical shifts (δ), quoted in parts per million (ppm), and coupling constants (J) were recorded in Hertz (Hz). All NMR spectra were recorded in deuterated chloroform or 1,1,2,2-tetrachloroethane ($CDCl_3$ or $C_2D_2Cl_4$) and solvent containing 0.003% TMS as an internal reference. The molecular weight and molecular weight distribution of the synthesized polymers were measured with a Waters GPC (Breeze system) using tetrahydofuran (THF) as an eluent at 35 °C. The apparatus was equipped with two Waters Styragel columns (HR3 and HR4E), a refractive index detector (Waters 2414), and a dual-wavelength absorbance detector (Waters 2487). Polystyrene standards (Waters) were used for calibration. Cyclic voltammetry (CV) was performed on an Autolab PGSTAT 30 Electrochemical Workstation with a three-electrode system in a solution of 0.1 M tetrabutylammonium perchlorate (Bu_4NClO_4) in deoxygenated acetonitrile (CH_3CN) at a scan rate of 50 mV s^{-1}. The polymer films were coated on working electrodes of the ITO sheet by solvent casting. A platinum wire was used as the counter electrode, and a silver wire was used as a quasi-reference electrode. The potential of the as-prepared polymer was corrected by the standard reference of Fc/Fc^+ in CH_3CN (0.45 V vs Ag/Ag^+ electrode), where the absolute energy level of ferrocene is −4.8 eV below the vacuum level. The HOMO and LUMO energy levels of the polymer were calculated according to the equation

$$E_{HOMO} = -(E_{ox}^{onset} + 4.35)\ eV$$

and

$$E_{LUMO} = -(E_{red}^{onset} + 4.35)\ eV$$

in which E_{ox}^{onset} and E_{red}^{onset} are the onset potentials for the oxidation and reduction processes, respectively.[17] TM-AFM images were taken on a NanoScope IIIa controller (Veeco Metrology Group/Digital Instruments, Santa Barbara, CA), using a built-in software (version V6.13R1) to capture images. X-ray diffraction (XRD) pattern was collected using a Rigaku-TTRAX III diffractometer, operating at an accelerating voltage of 50 kV and current of 300 mA. A nickel (Ni)-filtered Cu Kα radiation source (0.154 nm) was used. A scanning rate of 4° min^{-1} and a scanning range of ∼1.5°−40° 2θ were carefully chosen to allow for complete X-ray penetration into the powdery **PBDT-TFQ** film. The absorption spectra were obtained on a Hitachi U-4100 spectrophotometer. Hole mobility was measured according to a similar method described in the literature,[18] using a diode configuration of ITO/PEDOT:PSS/polymer: $PC_{71}BM$/Pd. The SCLC current was measured under dark conditions using a Keithley Model 2400 source meter.

Solar Cell Device Fabrication and Characterization. Optimized solar cell devices used in this study were prepared by dissolving **PBDT-TFQ** and $PC_{71}BM$ (purchased from Nano-C) in 1,2-dichlorobenzene (DCB) in the weight ratios of 1:0.5, 1:1, and 1:2 with a **PBDT-TFQ** concentration of 10 mg mL^{-1}. For device fabrication, solution was stirred for more than 12 h to ensure complete dissolution. Patterned indium tin oxide (ITO)-coated glass substrates (Kintec Company, 15 Ω/□) were successively cleaned by ultrasonication in 1% neutral detergent in water, followed by deionized water, then acetone, and finally ethanol for 20 min each. The substrates were then dried and O_2 plasma cleaned immediately prior to the deposition of a 40-nm-thick layer of aqueous PEDOT:PSS PH500 (H.C. Starck) solution, as verified by a Filmetrics Model F10-RT-UV system. Deposition of the PEDOT:PSS layer was followed by baking at 140 °C for 20 min. Substrates were subsequently transferred to an inert N_2-filled glovebox (<0.1 ppm O_2 and H_2O), and the active layer was spin-coated. The wet film was slowly dried in a covered Petri dish for a certain time and subsequently annealed at 140 °C for 10 min in the glovebox. The thicknesses of the **PBDT-TFQ**:$PC_{71}BM$ composite films were adjusted to ∼90−160 nm by controlling the spin-coating rates with two steps. The coated substrates were then transferred to a thermal evaporator and evacuated to ≤1 × 10^{-6} Torr before a 30-nm-thick calcium layer, followed by a 100-nm aluminum electrode layer were deposited. The active area of each device was 0.04 cm^2 with a length:width ratio of 1:1. The fabricated device was encapsulated in a nitrogen-filled glovebox with UV epoxy and cover glass. The J−V curves were measured with a Newport−Oriel (Sol3A Class AAA Solar Simulators) AM 1.5G light source operating at 100 mW cm^{-2}, and independently cross-checked using a 300-W AM 1.5G source operating at 100 mW cm^{-2} for verification. The light intensity was determined by a monosilicon detector (with KG-5 visible color filter) calibrated by the National Renewable Energy Laboratory (NREL) to minimize spectral mismatch. A 0.20 cm × 0.20 cm shadow mask was used to cover the active area for avoiding interference from both scattering light and adjacent current leakage. The IPCE spectra were measured using a lock-in amplifier with a current preamplifier under short-circuit conditions. The devices were illuminated by monochromatic light from a xenon lamp passing through a monochromator with a typical intensity of 30 μW. A calibrated monosilicon diode with known spectral response was used as a reference.

dx.doi.org/10.1021/cm302861s | *Chem. Mater.* 2012, 24, 4766−4772

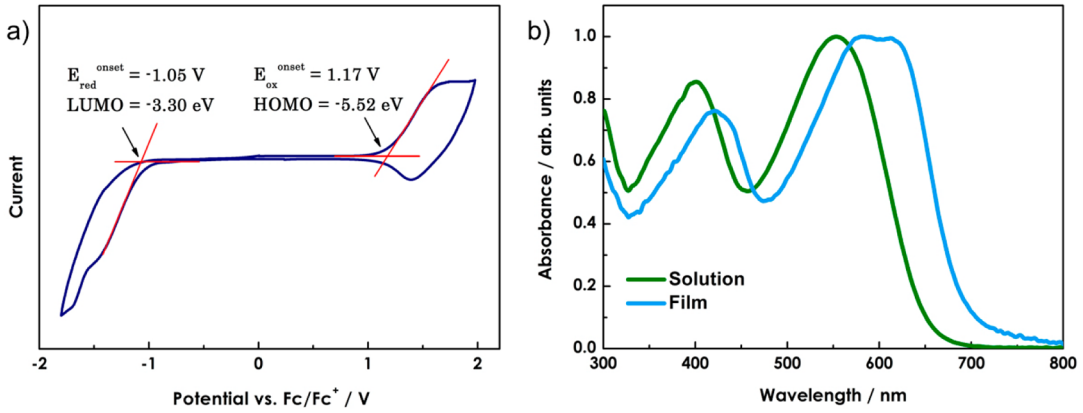

Figure 1. (a) Cyclic voltammogram of **PBDT-TFQ** in the thin film at a scan rate of 50 mV s^{-1}. (b) UV−vis absorption spectra of **PBDT-TFQ** in 1,2-dichlorobenzene solution and as a film.

RESULTS AND DISCUSSION

On the basis of the D-A concept, the medium electron-donating BDT moiety and strong electron-accepting TFQ unit were utilized to synthesize the medium-band gap **PBDT-TFQ** copolymer. The synthesis routes of the monomers and corresponding polymer are illustrated in Scheme 1. The copolymer **PBDT-TFQ** was obtained by a Stille cross-coupling polymerization of 2BrTFQ with BDT using $Pd(PPh_3)_4$ as a catalyst via thermal heating, and was in good yield, as shown in the Supporting Information. **PBDT-TFQ** exhibits an excellent film-casting property, as well as great solubility in common halogenated solvents. The weight-average molecular weights (M_w) of **PBDT-TFQ** copolymers are 37 and 71 kg mol^{-1}, with polydispersity indexes (PDIs) of 3.27 and 1.54, respectively, as determined by gel permeation chromatography (GPC) using THF as an eluent calibrated with polystyrene standards. Thermal stability of the polymer was confirmed by thermogravimetric analysis (TGA) at a temperature ramp rate of 10 °C min^{-1} under N_2 (see Figure S12 in the Supporting Information). The onset decomposition temperature of **PBDT-TFQ** at 5% weight loss is 333 °C, indicating high thermal stability of the as-prepared polymer.

The HOMO and LUMO energy levels of **PBDT-TFQ** were calculated by cyclic voltammogram (CV) from the onset potential of the first oxidation and reduction peaks shown in Figure 1a. The corresponding HOMO and LUMO energy levels of **PBDT-TFQ** were determined to be −5.52 and −3.30 eV, respectively. **PBDT-TFQ** exhibits a deeply low-lying HOMO energy level, which is in an ideal range to ensure better air stability and can be anticipated to approach high V_{oc}, in accordance with the linear correlation of the difference between the HOMO energy level of a donor polymer and the LUMO energy level of an acceptor.[13] Indeed, the introduction of electron-deficient F atoms can further lower both the HOMO and LUMO energy levels, and the result agrees well with the previous reports.[1b,3a,10a,b,14] Therefore, the relatively low-lying HOMO level and small band gap, along with good solubility, favorable geometry, and promising charge carrier transportation, could act as an effective donor component for BHJ solar cells (vide infra). Considering the LUMO level of $PC_{71}BM$ is located at −4.02 eV,[2b] the offset between donor polymer and acceptor $PC_{71}BM$ should provide an enough driving force for efficient exciton dissociation, ensuring energetically favorable electron transfer.[1a] As shown in Figure 1b, **PBDT-TFQ** in dilute DCB solution exhibits a broad and strong absorption spectral feature across the entire UV−vis region, with two absorption bands located at 401 and 553 nm. The shorter wavelength peak is assigned to the localized $\pi-\pi^*$ transitions, whereas the lower energy band corresponds to the ICT between D and A moieties. In film, the absorption becomes broader and is significantly red-shifted with three peaks at ∼421, 583, and 612 nm, respectively. The large red-shift is observed in the absorption maxima (λ_{max}) relative to dilute solution as a result of a more planar polymer chain structure and/or the degree of interchain π-stacking in the solid film. Such ordered packing of polymer chains is beneficial for improving the charge carrier mobility of resulting films. Furthermore, the absorption edge (λ_{edge}) of **PBDT-TFQ** film is 718 nm, from which the E_g^{opt} value for **PBDT-TFQ**, deduced from the onset of absorption in the solid state, is determined to be 1.73 eV (Table 1).

Table 1. Optical and Electrochemical Properties of PBDT-TFQ

	λ_{max} [nm]		λ_{edge} [nm]				
polymer	solution	film	film	HOMO [eV][a]	LUMO [eV][a]	E_g^{EC} [eV][b]	E_g^{opt} [eV][c]
PBDT-TFQ	401, 553	421, 583, 612	718	−5.52	−3.30	2.22	1.73

[a]HOMO and LUMO levels were estimated from the onset of the oxidation and reduction peaks of cyclic voltammogram. [b]Electrochemical band gap calculated from cyclic voltammogram. [c]Optical band gap estimated from the onset of UV−vis spectrum of the film.

BHJ solar cells based on the **PBDT-TFQ** polymer were fabricated in a typical configuration of ITO/PEDOT:PSS/polymer:$PC_{71}BM$ (1:0.5, 1:1, and 1:2, w/w)/Ca/Al and tested. PSCs were optimized empirically by scrutinizing variations in the molecular weight of the polymer, the polymer concentrations, the blend ratios of the polymer to $PC_{71}BM$, the choice of solvent, the processing additives, the spin speed, and the thermal treatment. More than 200 devices have been fabricated in total, and the optimized blend ratio was 1:1. The resulting J_{sc}, V_{oc}, FF, and PCE values were determined from the $J-V$ curves, and all of the relevant solar cell parameters are summarized in Table 2. It is worth noting that **PBDT-TFQ**-based devices did not perform optimally when spin-casted from pristine (DCB) solvent and thus required the use of a processing additive. 1,8-

dx.doi.org/10.1021/cm302861s | Chem. Mater. 2012, 24, 4766−4772

Table 2. Representative Photovoltaic Performance for PBDT-TFQ:$PC_{71}BM$ Devices under AM 1.5G Solar Illumination

device	D/A ratio	solvent	V_{oc} [V]	J_{sc} [mA cm^{-2}]	FF [%]	PCE_{ave} [%][b]	thickness [nm][c]
D1	1:0.5	DCB	0.86 ± 0.01	10.3 ± 0.5	46.8 ± 0.3	4.2 ± 0.2 (4.4)	96
D2	1:0.5	DCB + 3% DIO	0.81 ± 0.01	14.2 ± 0.2	53.7 ± 0.9	6.2 ± 0.2 (6.4)	90
D3	1:1	DCB	0.82 ± 0.01	12.3 ± 0.8	49.1 ± 0.2	4.9 ± 0.4 (5.3)	100
D4	1:1	DCB + 3% DIO	0.78 ± 0.01	15.5 ± 0.6	56.8 ± 0.7	6.9 ± 0.3 (7.2)	93
D5[a]	1:1	DCB + 3% DIO	0.76 ± 0.01	17.9 ± 0.3	57.6 ± 0.5	7.8 ± 0.2 (8.0)	106
D6	1:2	DCB	0.83 ± 0.02	7.91 ± 0.8	45.1 ± 0.3	3.0 ± 0.4 (3.4)	123
D7	1:2	DCB + 3% DIO	0.80 ± 0.01	12.9 ± 0.7	54.5 ± 0.3	5.6 ± 0.4 (6.0)	112

[a]High-molecular-weight **PBDT-TFQ**. [b]Only the optimized recipes were considered for the estimation of the average PCE; data have been averaged over 10 devices; the performance of the best device is given in parentheses. [c]Thickness of the active layers.

Diiodooctane (DIO) was used as the additive, because of its high boiling point (168 °C) and ability to solvate the fullerenes, leading to a comprehensive impact on J_{sc} by providing more optimal morphology for facilitating charge carrier transportation.[7a,15] However, it was found that the addition of DIO to the active layers tends to drop the V_{oc} of the devices to some extent. This reduction can be attributed to the lowering of charge-separated and charge-transfer-state energies upon additive addition.[16] Overall, devices with 3% DIO additive exhibit better PCEs than that of the devices without any additive (see Figure S14 in the Supporting Information). In the **PBDT-TFQ**-based devices, the 1:1 blends outperformed the 1:0.5 and 1:2 blends. Aside from the blend ratios, however, they all showed high performance, with average PCEs above 5.6% under AM 1.5G illumination, which facilitates the preparation of high-performance solar cells. With a weight ratio of 1:1 **PBDT-TFQ**:$PC_{71}BM$, a high V_{oc} of 0.78 V was observed. This, combined with a high J_{sc} of 15.5 mA cm^{-2}, and FF = 56.8%, results in an average PCE of 6.9% under AM 1.5G irradiation. Moreover, the device was further upgraded to 7.8% (average), along with the highest PCE of 8.0% (V_{oc} = 0.76 V, J_{sc} = 18.2 mA cm^{-2}, and FF = 58.1%) by utilization of a high-molecular-weight **PBDT-TFQ** (71 kg mol^{-1}), and it showed substantial improvement in J_{sc} and FF, in comparison to that made with a moderate molecular weight of **PBDT-TFQ** (37 kg mol^{-1}) at the same blend ratio, as depicted in Figure 2a. Moreover, the corresponding D/A blend ratio dependency of the photovoltaic parameters, the V_{oc}, J_{sc}, FF, and PCE data are shown in Figure 3. The superior performance of the high-molecular-weight **PBDT-TFQ**-based solar cells is associated with the high hole mobility and better nanoscale morphology of the interpenetrating network (vide infra), allowing efficient exciton dissociation and enhancing charge carrier transportation. The above encapsulated devices were then sent to Center for Measurement Standards located at Industrial Technology Research Institute (ITRI) of Taiwan for further certification. The corresponding PSCs certifications are shown in Figures S15 and S16 in the Supporting Information). Certified PCEs of 7.3% and 6.3% for the devices with high-molecular-weight and moderate-molecular-weight **PBDT-TFQ**, respectively, are observed under 1 sun, AM 1.5G illumination. Comparing these values with those measured in our laboratory, we found an ∼9% drop in both certified PCEs, which mainly resulted from the reduction in J_{sc} and FF. The degradation of certified PSCs can be attributed to the nonoptimized encapsulation process, together with the significant time delay between sending the devices to ITRI and with the queuing time of the ITRI measurement. Nevertheless, note that **PBDT-TFQ**-based high-performance solar cells were accomplished via a simple

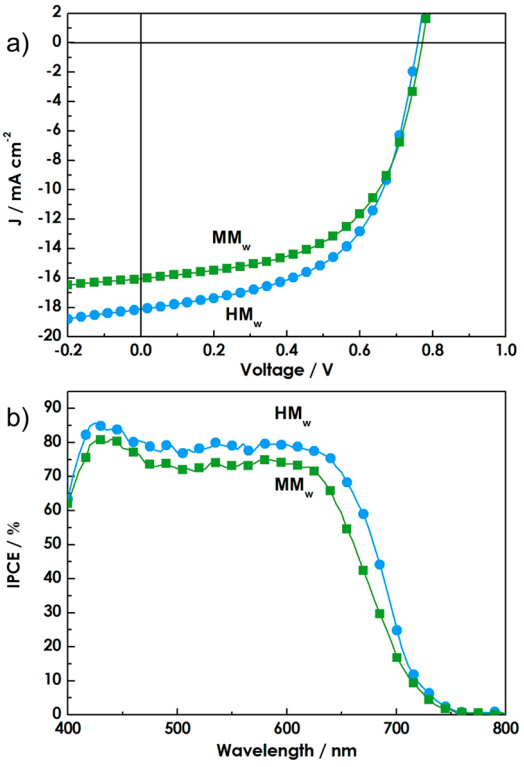

Figure 2. (a) $J-V$ curves of 1:1 **PBDT-TFQ**:$PC_{71}BM$ solar cells with high-molecular-weight (HM_w) and moderate-molecular-weight (MM_w) **PBDT-TFQ** under AM 1.5G solar illumination, and (b) corresponding IPCE spectra of optimized 1:1 **PBDT-TFQ**:$PC_{71}BM$ devices made from HM_w and MM_w of **PBDT-TFQ** illuminated by monochromatic light. Legend: light blue circles (●) represent the HM_w device (V_{oc} = 0.76 V, J_{sc} = −18.2 mA cm^{-2}, FF = 58.1%, and PCE = 8.0%) and olive green squares (■) represent the MM_w device (V_{oc} = 0.78 V, J_{sc} = −16.1 mA cm^{-2}, FF = 57.5%, and PCE = 7.2%).

fabrication configuration without additional modified layers, which is advisable for cost-effective PSCs.

The incident photon-to-current efficiency (IPCE) of the solar cells was measured under the illumination of monochromatic light. For the PSC devices fabricated from the 1:1 **PBDT-TFQ**:$PC_{71}BM$ blend with high-molecular-weight and moderate-molecular-weight **PBDT-TFQ**, very broad panchromatic spectra over the entire excitation spectral range were obtained from IPCE measurements, as illustrated in Figure 2b. The optimum device very efficiently harvests solar light in the maximum IPCE of 85.5% at 425 nm, and exhibits a broad photoresponse of over 75% in the 407−640-nm range. The calculated J_{sc} values of 1:1 **PBDT-TFQ**:$PC_{71}BM$ devices with high-molecular-weight and moderate-molecular-weight **PBDT-**

dx.doi.org/10.1021/cm302861s | *Chem. Mater.* 2012, 24, 4766−4772

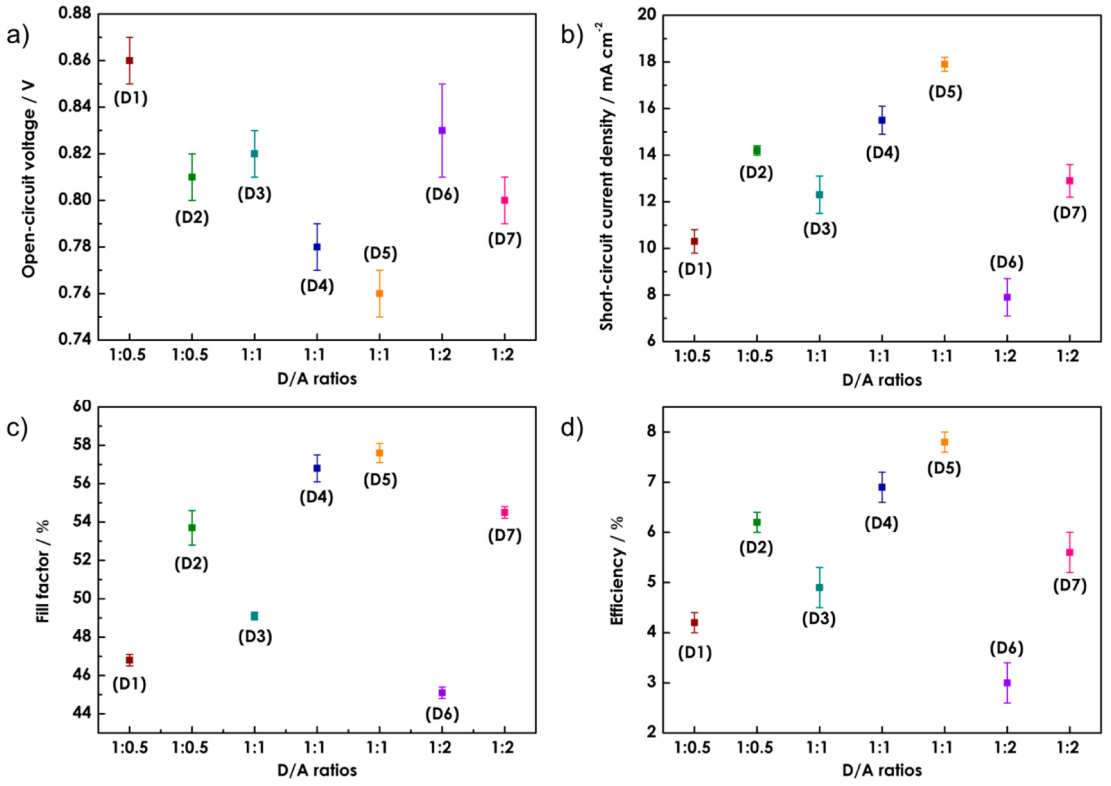

Figure 3. Photovoltaic parameters of the corresponding PSCs under AM 1.5G solar illumination: (a) open-circuit voltage, (b) short-circuit current density, (c) fill factor, and (d) power conversion efficiency as a function of D/A blend ratios.

TFQ from IPCE curves are 16.3 and 14.6 mA cm^{-2}, respectively, which confirm the high J_{sc} values of the devices. The J_{sc} mismatch could be ascribed to the following reasons:

(1) As measured by the IPCE instrument, <5%−10% error in spectral mismatch would take place.[1a]

(2) Our IPCE instrument resolution below 400 nm is less accurate. Regarding this compound, the spectral response below 400 nm still has absorption and, thus, may be reflected in part to the slight loss in IPCE spectra.

It is also clear that **PBDT-TFQ** devices exhibited distinguished improvement across the entire photoresponse region with increased **PBDT-TFQ** molecular weight, indicating that the enhancement in J_{sc} resulted from the more-efficient exciton dissociation and the robust charge collection from both the **PBDT-TFQ** and $PC_{71}BM$ domains. Furthermore, the results also demonstrate that the solar energy response for the current generation extends to 750 nm, as expected from the absorption spectrum of the active layer (see Figure S17 in the Supporting Information).

In consideration of charge-carrier mobilities in blend films, hole-only devices in a configuration of ITO/PEDOT:PSS/active layer/Pd were measured by using the space-charge-limited current (SCLC) model at low voltage.[18] The device characteristics were extracted by modeling the dark current under forward bias, described by the Mott−Gurney law. For comparison, the hole mobility of 1:1 **PBDT-TFQ**:$PC_{71}BM$ devices varied from 3.8×10^{-4} cm^2 V^{-1} s^{-1} to 2.3×10^{-3} cm^2 V^{-1} s^{-1} as the molecular weight of **PBDT-TFQ** increased from 37 kg mol^{-1} to 71 kg mol^{-1} shown in Figure 4. There was a difference of ~6 times in mobility between the devices with high-molecular-weight and moderate-molecular-weight **PBDT-TFQ**. The higher hole mobility yielded a balanced charge

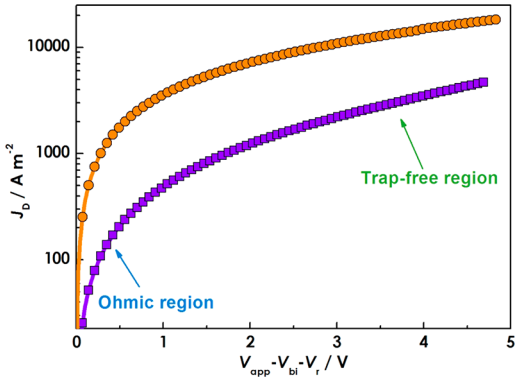

Figure 4. Determination of the hole mobility from the dark current densities for **PBDT-TFQ**:$PC_{71}BM$ (1:1) diodes with high-molecular-weight **PBDT-TFQ** (denoted by orange circles, ●) and moderate-molecular-weight **PBDT-TFQ** (denoted by purple squares, ■).

carrier transport in the active layer, which is expected to contribute in part to the high J_{sc} and FF values observed in optimized BHJ devices (Figure 2a).

The charge-carrier mobility and the nanoscale morphology of the BHJ film are the two major factors that could be significantly affected by the polymer molecular weight. Tapping-mode atomic force microscopy (TM-AFM) studies were conducted to investigate the film morphology of the **PBDT-TFQ**:$PC_{71}BM$ (1:1) active layers with and without DIO additive after thermal annealing at 140 °C for 10 min. The 1:1 blend film exhibits unevenly aggregated polymer and $PC_{71}BM$ domains, forming large islands ~100 nm in diameter and a root-mean-square (rms) roughness of 3.10 nm (see Figure 5). Consequently, this adverse morphology reduces the effective

dx.doi.org/10.1021/cm302861s | *Chem. Mater.* 2012, 24, 4766−4772

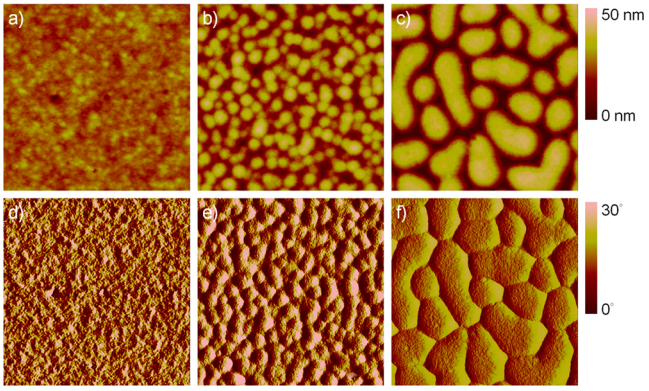

Figure 5. Morphology characterization of (a–c) TM-AFM topography and (d–f) phase images of **PBDT-TFQ**:$PC_{71}BM$ blend films with various compositions: (panels a and d) 1:0.5, (panels b and e) 1:1, and (panels c and f) 1:2. The imaging size is 2 μm × 2 μm for each panel.

D/A interface and thus limits the exciton dissociation probability, resulting in exciton loss, geminate charge recombination, and poor charge mobility.[7e] In contrast, addition of a small amount of additive to the blend film results in smoother (rms roughness of 2.01 nm) surfaces without large domains (very fine domains ~10 nm in size), as shown in Figures 6a and 6c. It is noteworthy that the blend film based on

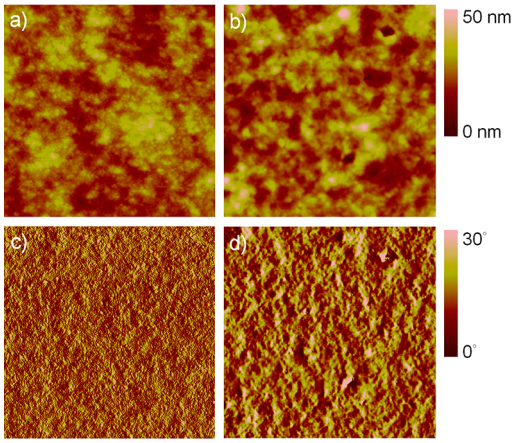

Figure 6. TM-AFM topography images (upper row) and phase images (lower row) of **PBDT-TFQ**:$PC_{71}BM$ (1:1) blend films with 3% DIO from (panels a and c) moderate-molecular-weight **PBDT-TFQ** and (panels b and d) high-molecular-weight **PBDT-TFQ**. The imaging size is 2 μm × 2 μm in each panel.

a high-molecular-weight **PBDT-TFQ** tends to form an interpenetrating bicontinuous network structure (rms roughness of 2.49 nm), because of the enhancement of continual π-conjugated lengths of polymer chains, and thus develops highly dense interconnections within the interpenetrating network for optimal charge generation and transport, as shown in Figures 6b and 6d. The result is consistent with previous reports.[1d,3c,e] These TM-AFM results are also consistent with the corresponding photovoltaic device performances (vide supra). The prominent J_{sc} value implies that the morphology of nanoscale phase separation within the polymer blend enables a large interface area and a finer bicontinuous structure of both domains with widths of 10–20 nm, which is closely related to the ideal value for efficient exciton dissociation. Therefore, the relatively high hole mobility together with the excellent morphology mentioned above, results in a high J_{sc} and FF.

CONCLUSIONS

In summary, we have designed and synthesized a new medium-band gap conjugated polymer of **PBDT-TFQ**, and we have demonstrated excellent photon harvesting and efficient photogeneration of charge-separated states when it is blended with $PC_{71}BM$. The resulting copolymer revealed the desired deep HOMO and LUMO energy levels, allowing high V_{oc} and J_{sc} values. Moreover, the high charge carrier mobility and better continuous percolation pathways for charge transport lead to a superior power conversion efficiency (PCE) of up to 8.0%, which applies to a high-performance polymer solar cell (PSC). The prospect of its future extension is promising; this includes optimization of the molecular weight of **PBDT-TFQ**, rational chemical modification, and engineering the interfacial layers and device architectures in an effort to achieve record performance.

ASSOCIATED CONTENT

Supporting Information

Details for the synthesis and characterization of **PBDT-TFQ** copolymer and experimental protocols for the devices are given in the Supporting Information. This material is available free of charge via the Internet at http://pubs.acs.org.

AUTHOR INFORMATION

Corresponding Author

*E-mail addresses: austinchen@ntu.edu.tw (H.-C.C.), chop@ntu.edu.tw (P.-T.C.).

Notes

The authors declare no competing financial interest.

ACKNOWLEDGMENTS

We gratefully acknowledge the financial support of this work by the National Science Council and Ministry of Economic Affairs of Taiwan. We also thank Dr. I-Wen P. Chen and Prof. Chun-hsien Chen, National Taiwan University, for the TM-AFM support.

REFERENCES

(1) (a) Thompson, B. C.; Fréchet, J. M. J. *Angew. Chem., Int. Ed.* **2008**, *47*, 58–77. (b) Price, S. C.; Stuart, A. C.; Yang, L.; Zhou, H.; You, W. *J. Am. Chem. Soc.* **2011**, *133*, 4625–4631. (c) Li, G.; Zhu, R.; Yang, Y. *Nat. Photonics* **2012**, *6*, 153–161. (d) Müller, C.; Wang, E.; Andersson, L. M.; Tvingstedt, K.; Zhou, Y.; Andersson, M. R.; Inganäs, O. *Adv. Funct. Mater.* **2010**, *20*, 2124–2131. (e) Lee, D.; Hubijar, E.; Kalaw, G. J. D.; Ferraris, J. P. *Chem. Mater.* **2012**, *24*, 2534–2540. (f) Duan, R.; Ye, L.; Guo, X.; Huang, Y.; Wang, P.; Zhang, S.; Zhang, J.; Huo, L.; Hou, J. *Macromolecules* **2012**, *45*, 3032–3038.

(2) (a) Iyer, A.; Bjorgaard, J.; Anderson, T.; Köse, M. E. *Macromolecules* **2012**, *45*, 6380–6389. (b) Chen, H.-C.; Wu, I.-C.; Hung, J.-H.; Chen, F.-J.; Chen, I-W. P.; Peng, Y.-K.; Lin, C.-S.; Chen, C.-h.; Sheng, Y.-J.; Tsao, H.-K.; Chou, P.-T. *Small* **2011**, *7*, 1098–1107. (c) Du, C.; Li, C.; Li, W.; Chen, X.; Bo, Z.; Veit, C.; Ma, Z.; Wuerfel, U.; Zhu, H.; Hu, W.; Zhang, F. *Macromolecules* **2011**, *44*, 7617–7624. (d) Tang, Z.; Andersson, L. M.; George, Z.; Vandewal, K.; Tvingstedt, K.; Heriksson, P.; Kroon, R.; Andersson, M. R.; Inganäs, O. *Adv. Mater.* **2012**, *24*, 554–558. (e) Chan, S.-H.; Lai, C.-S.; Chen, H.-L.; Ting, C.; Chen, C.-P. *Macromolecules* **2011**, *44*, 8886–8891. (f) Kroon, R.; Gehlhaar, R.; Steckler, T. T.; Henriksson, P.; Müller, C.; Bergqvist, J.; Hadipour, A.; Heremans, P.; Andersson, M. R. *Sol. Energy Mater. Sol. Cells* **2012**, *105*, 280–286.

(3) (a) Son, H. J.; Wang, W.; Xu, T.; Liang, Y.; Wu, Y.; Li, G.; Yu, L. *J. Am. Chem. Soc.* **2011**, *133*, 1885−1894. (b) Huo, L.; Guo, X.; Zhang, S.; Li, Y.; Hou, J. *Macromolecules* **2011**, *44*, 4035−4037. (c) Tong, M.; Cho, S.; Rogers, J. T.; Schmidt, K.; Hsu, B. B. Y.; Moses, D.; Coffin, R. C.; Kramer, E. J.; Bazan, G. C.; Heeger, A. J. *Adv. Funct. Mater.* **2010**, *20*, 3959−3965. (d) Subramaniyan, S.; Xin, H.; Kim, F. S.; Jenekhe, S. A. *Macromolecules* **2011**, *44*, 6245−6248. (e) Chu, T.-Y.; Lu, J.; Beaupré, S.; Zhang, Y.; Pouliot, J.-R.; Zhou, J.; Najari, A.; Leclerc, M.; Tao, Y. *Adv. Funct. Mater.* **2012**, *22*, 2345−2351.

(4) (a) Backer, S. A.; Sivula, K.; Kavulak, D. F.; Fréchet, J. M. J. *Chem. Mater.* **2007**, *19*, 2927−2929. (b) He, Y.; Chen, H.-Y.; Hou, J.; Li, Y. *J. Am. Chem. Soc.* **2010**, *132*, 1377−1382. (c) Lenes, M.; Wetzelaer, G.-J. A. H.; Kooistra, F. B.; Veenstra, S. C.; Hummelen, J. C.; Blom, P. W. M. *Adv. Mater.* **2008**, *20*, 2116−2119. (d) Kim, K.-H.; Kang, H.; Nam, S. Y.; Jung, J.; Kim, P. S.; Cho, C.-H.; Lee, C.; Yoon, S. C.; Kim, B. J. *Chem. Mater.* **2011**, *23*, 5090−5095. (e) Kim, K.-H.; Kang, H.; Kim, H. J.; Kim, P. S.; Yoon, S. C.; Kim, B. J. *Chem. Mater.* **2012**, *24*, 2373−2381.

(5) (a) Chen, H.-C.; Lai, C.-W.; Wu, I.-C.; Pan, H.-R.; Chen, I-W. P.; Peng, Y.-K.; Liu, C.-L.; Chen, C.-h.; Chou, P.-T. *Adv. Mater.* **2011**, *23*, 5451−5455. (b) Greaney, M. J.; Das, S.; Webber, D. H.; Bradforth, S. E.; Brutchey, R. L. *ACS Nano* **2012**, *6*, 4222−4230. (c) Zhang, H.; Liu, Y.; Yao, D.; Yang, B. *Chem. Soc. Rev.* **2012**, *41*, 6066−6088. (d) Wei, H.; Zhang, H.; Sun, H.; Yang, B. *Nano Today* **2012**, *7*, 316−326. (e) Yuan, K.; Li, F.; Chen, L.; Li, Y.; Chen, Y. *J. Phys. Chem. C* **2012**, *116*, 6332−6339.

(6) (a) Choi, H.; Park, J. S.; Jeong, E.; Kim, G.-H.; Lee, B. R.; Kim, S. O.; Song, M. H.; Woo, H. Y.; Kim, J. Y. *Adv. Mater.* **2011**, *23*, 2759−2763. (b) Cheng, Y.-J.; Hsieh, C.-H.; Li, P.-J.; Hsu, C.-S. *Adv. Funct. Mater.* **2011**, *21*, 1723−1732. (c) Cheng, Y.-J.; Cao, F.-Y.; Lin, W.-C.; Chen, C.-H.; Hsieh, C.-H. *Chem. Mater.* **2011**, *23*, 1512−1518. (d) Ma, H.; Yip, H.-L.; Huang, F.; Jen, A. K.-Y. *Adv. Funct. Mater.* **2010**, *20*, 1371−1388. (e) Sun, Y.; Seo, J. H.; Takacs, C. J.; Seifter, J.; Heeger, A. J. *Adv. Mater.* **2011**, *23*, 1679−1683.

(7) (a) Peet, J.; Kim, J. Y.; Coates, N. E.; Ma, W. L.; Moses, D.; Heeger, A. J.; Bazan, G. C. *Nat. Mater.* **2007**, *6*, 497−500. (b) Wang, D. H.; Kim, D. Y.; Choi, K. W.; Seo, J. H.; Im, S. H.; Park, J. H.; Park, O O.; Heeger, A. J. *Angew. Chem., Int. Ed.* **2011**, *50*, 5519−5523. (c) Kim, Y. H.; Sachse, C.; Machala, M. L.; May, C.; Müller-Meskamp, L.; Leo, K. *Adv. Funct. Mater.* **2011**, *21*, 1076−1081. (d) Lai, Y.-C.; Higashihara, T.; Hsu, J.-C.; Ueda, M.; Chen, W.-C. *Sol. Energy Mater. Sol. Cells* **2012**, *97*, 164−170. (e) Chen, H.-C.; Chou, S.-W.; Tseng, W.-H.; Chen, I-W. P.; Liu, C.-C.; Liu, C.; Liu, C.-L.; Chen, C.-h.; Wu, C.-I; Chou, P.-T. *Adv. Funct. Mater.* **2012**, *22*, 3975−3984.

(8) (a) Lunt, R. R.; Osedach, T. P.; Brown, P. R.; Rowehl, J. A.; Bulović, V. *Adv. Mater.* **2011**, *23*, 5712−5727. (b) Dou, L.; You, J.; Yang, J.; Chen, C.-C.; He, Y.; Murase, S.; Moriarty, T.; Emery, K.; Li, G.; Yang, Y. *Nat. Photonics* **2012**, *6*, 180−185. (c) Jørgensen, M.; Norrman, K.; Gevorgyan, S. A.; Tromholt, T.; Andreasen, B.; Krebs, F. C. *Adv. Mater.* **2012**, *24*, 580−612. (d) Gevaerts, V. S.; Furlan, A.; Wienk, M. M.; Turbiez, M.; Janssen, R. A. J. *Adv. Mater.* **2012**, *24*, 2130−2134.

(9) (a) Kitamura, C.; Tanaka, S.; Yamashita, Y. *Chem. Mater.* **1996**, *8*, 570−578. (b) Jenekhe, S. A.; Lu, L.; Alam, M. M. *Macromolecules* **2001**, *34*, 7315−7324.

(10) (a) Chen, H.-Y.; Hou, J.; Zhang, S.; Liang, Y.; Yang, G.; Yang, Y.; Yu, L.; Wu, Y.; Li, G. *Nat. Photonics* **2009**, *3*, 649−653. (b) Zhou, H.; Yang, L.; Stuart, A. C.; Price, S. C.; Liu, S.; You, W. *Angew. Chem., Int. Ed.* **2011**, *50*, 2995−2998. (c) Huo, L.; Hou, J.; Zhang, S.; Chen, H.-Y.; Yang, Y. *Angew. Chem., Int. Ed.* **2010**, *49*, 1500−1503. (d) Chu, T.-Y.; Lu, J.; Beaupré, S.; Zhang, Y.; Pouliot, J.-R.; Wakim, S.; Zhou, J.; Leclerc, M.; Li, Z.; Ding, J.; Tao, Y. *J. Am. Chem. Soc.* **2011**, *133*, 4250−4253. (e) He, Z.; Zhong, C.; Huang, X.; Wong, W.-Y.; Wu, H.; Chen, L.; Su, S.; Cao, Y. *Adv. Mater.* **2011**, *23*, 4636−4643. (f) Liang, Y.; Xu, Z.; Xia, J.; Tsai, S.-T.; Wu, Y.; Li, G.; Ray, C.; Yu, L. *Adv. Mater.* **2010**, *22*, E135−E138. (g) Amb, C. M.; Chen, S.; Graham, K. R.; Subbiah, J.; Small, C. E.; So, F.; Reynolds, J. R. *J. Am. Chem. Soc.* **2011**, *133*, 10062−10065.

(11) (a) Pan, H.; Li, Y.; Wu, Y.; Liu, P.; Ong, B. S.; Zhu, S.; Xu, G. *Chem. Mater.* **2006**, *18*, 3237−3241. (b) Pan, H.; Wu, Y.; Li, Y.; Liu, P.; Ong, B. S.; Zhu, S.; Xu, G. *Adv. Funct. Mater.* **2007**, *17*, 3574−3579.

(12) (a) Li, Z.; Zhang, Y.; Tsang, S.-W.; Du, X.; Zhou, J.; Tao, Y.; Ding, J. *J. Phys. Chem. C* **2011**, *115*, 18002−18009. (b) Piliego, C.; Holcombe, T. W.; Douglas, J. D.; Woo, C. H.; Beaujuge, P. M.; Fréchet, J. M. J. *J. Am. Chem. Soc.* **2010**, *132*, 7595−7597.

(13) Brabec, C. J.; Cravino, A.; Meissner, D.; Sariciftci, N. S.; Fromherz, T.; Rispens, M. T.; Sanchez, L.; Hummelen, J. C. *Adv. Funct. Mater.* **2001**, *11*, 374−380.

(14) (a) Reichenbächer, K.; Süss, H. I.; Hulliger, J. *Chem. Soc. Rev.* **2005**, *34*, 22−30. (b) Pagliaro, M.; Ciriminna, R. *J. Mater. Chem.* **2005**, *15*, 4981−4991.

(15) Lee, J. K.; Ma, W. L.; Brabec, C. J.; Yuen, J.; Moon, J. S.; Kim, J. Y.; Lee, K.; Bazan, G. C.; Heeger, A. J. *J. Am. Chem. Soc.* **2008**, *130*, 3619−3623.

(16) Nuzzo, D.; Di; Aguirre, A.; Shahid, M.; Gevaerts, V. S.; Meskers, S. C. J.; Janssen, R. A. J. *Adv. Mater.* **2010**, *22*, 4321−4324.

(17) (a) Miller, L. L.; Nordblom, G. D.; Mayeda, E. A. *J. Org. Chem.* **1972**, *37*, 916−918. (b) Yang, C. J.; Jenekhe, S. A. *Macromolecules* **1995**, *28*, 1180−1196.

(18) (a) Mihailetchi, V. D.; Koster, L. J. A.; Blom, P. W. M.; Melzer, C.; de Boer, B.; van Duren, J. K. J.; Janssen, R. A. J. *Adv. Funct. Mater.* **2005**, *15*, 795−801. (b) Mihailetchi, V. D.; Xie, H.; de Boer, B.; Koster, L. J. A.; Blom, P. W. M. *Adv. Funct. Mater.* **2006**, *16*, 699−708.